

# Summer-Winter Contrast in the Response of Precipitation Extremes to Climate Change over Northern Hemisphere Land

Andrew I. L. Williams<sup>1</sup> and Paul A. O'Gorman<sup>2</sup>

<sup>1</sup>Atmospheric, Oceanic and Planetary Physics, Department of Physics, University of Oxford, Oxford, UK,  
<sup>2</sup>Department of Earth, Atmospheric and Planetary Sciences, Massachusetts Institute of Technology,

Department of Earth, Atmospheric and Planetary Sciences, Massachusetts Institute of Technology,  
Cambridge, MA USA

Cambridge, MA, USA

## Key Points:

- Over Northern Hemisphere extratropical land, the projected fractional increase of precipitation extremes is weaker in summer than winter
- The summer-winter contrast is mostly driven by weakened extreme ascent in summer, which is correlated with decreased surface relative humidity
- The summer-winter contrast is also evident in observations of historical changes in daily precipitation extremes, consistent with CMIP5 models

15 **Abstract**

16 Climate models project a distinct seasonality to future changes in daily extreme precipitation.  
 17 In particular, models project that over land in the extratropical Northern Hemisphere the summer response is substantially weaker than the winter response in percentage terms.  
 18 Here we decompose the projected response into thermodynamic and dynamic contributions and show that the seasonal contrast arises due to a negative dynamic contribution in northern summer, and a positive dynamic contribution and an anomalously strong thermodynamic contribution in northern winter. The negative dynamic contribution in northern summer is due to weakened ascent and is strongly correlated with decreases in mean near-surface relative humidity. Finally, we show that the summer-winter contrast is also evident in observed trends of daily precipitation extremes in northern midlatitudes, which provides support for the contrast found in climate-model simulations.  
 26

27 **Plain Language Summary**

28 Extreme rainfall is a highly impactful aspect of the water cycle, and it is now well-established that global warming tends to increase the severity of extreme rainfall events.  
 29 However, while this increase holds robustly on global scales, there is significant uncertainty associated with understanding the response of extreme rainfall to warming in different regions of the world and in different seasons. Here we focus on understanding changes  
 30 in extreme rainfall in summer and winter over Northern Hemisphere extratropical land.  
 31 We find that global warming has a contrasting impact on extreme rainfall over this region depending on the season considered. In winter, there are large increases in extreme  
 32 rainfall with warming relative to the climatology, whereas in summer the changes are much  
 33 weaker. We use a simple, physics-based approach to decompose these changes into contributions from changes in temperature and changes in ascent. Our results show that the  
 34 contrasting seasonal response over this region is mostly due to decreases in extreme ascent with warming in summer, and that the ‘summer-winter’ contrast is already present  
 35 in observed changes of extreme rainfall since the mid-20<sup>th</sup> century.  
 36  
 37  
 38  
 39  
 40  
 41

42 **1 Introduction**

43 The impacts of extreme precipitation are felt acutely across the world with consequences ranging from floods and landslides (Kirschbaum et al., 2012) to changes in ecosystems (Knapp et al., 2008). Additionally, it is now well-understood that extreme precipitation events intensify overall on a global scale in response to global warming (Wehner et al., 2020; Kharin et al., 2013; O’Gorman, 2015). On regional scales however, the response of precipitation extremes to warming is uncertain, with some regions projected to experience changes in precipitation extremes which are much higher or lower than the global-mean intensification (Pfahl et al., 2017). Put together, this makes regional changes in extreme precipitation potentially one of the most impactful consequences of global warming. Thus, understanding historical and future changes in regional extreme precipitation important not only from a scientific perspective, but also for understanding the unequal impacts of climate change (Diffenbaugh & Burke, 2019). In addition, considering precipitation extremes in different seasons helps to clarify physical drivers and can also be important for impacts.  
 44  
 45  
 46  
 47  
 48  
 49  
 50  
 51  
 52  
 53  
 54  
 55  
 56

57 To understand projections of changes in precipitation extremes it is useful to decompose the changes into contributions from different physical drivers. One such approach  
 58 is to use the simple, physical scaling developed by O’Gorman and Schneider (2009a) which  
 59 relates the intensity of precipitation extremes,  $P_e$ , to the pressure vertical velocity ( $\omega_e$ )  
 60 and the vertical derivative of saturation specific humidity with respect to pressure as-  
 61 suming a moist adiabatic lapse rate ( $\frac{dq_s}{dp}|_{\theta^*}$ ),  
 62

$$P_e \sim - \left\{ \omega_e \left. \frac{dq_s}{dp} \right|_{\theta^*} \right\}, \quad (1)$$

where  $\{\cdot\}$  denotes a mass-weighted vertical integral over the troposphere,  $\omega_e$  is evaluated on the day of the extreme event, and  $\left. \frac{dq_s}{dp} \right|_{\theta^*}$  is evaluated using the temperature  $T_e$  on the day of the extreme event. Thus, when considering a change in precipitation extremes due to global warming,  $\delta P_e$ , we can decompose the change into a thermodynamic contribution associated with changes in  $T_e$  and a dynamic contribution associated with changes in extreme ascent  $\omega_e$ ,

$$\delta P_e \approx \delta P_{\text{thermodynamic}} + \delta P_{\text{dynamic}}. \quad (2)$$

Pfahl et al. (2017) recently showed that Eq. 1 successfully captures the present-day and future changes of precipitation extremes in simulations from the Coupled Model Intercomparison Project Phase 5, CMIP5, (Taylor et al., 2012) and thus is a good proxy for understanding and decomposing these future changes (Fig. S1). Pfahl et al. (2017) used Eq. 1 to decompose future regional changes in annual and seasonal maximum daily precipitation (hereafter, Rx1day) in the CMIP5 simulations into thermodynamic and dynamic contributions. The thermodynamic contribution is positive and relatively spatially uniform, whereas the dynamic contribution varies strongly between regions and seasons and can either locally amplify or counteract the increases from the thermodynamic contribution.

The results of Pfahl et al. (2017) show a pronounced ‘summer-winter’ contrast in the response of seasonal Rx1day. The fraction of Northern Hemisphere (NH) extratropical land experiencing robust increases is relatively small in June-July-August (JJA), due to a negative dynamic contribution over land, particularly over Europe and North America. Similar results were found by Tandon et al. (2018) for the CanESM2 large ensemble. By contrast, Pfahl et al. (2017) found a strong response of precipitation extremes in the NH extratropics for December-January-February (DJF), and climate change was found to induce a shift in precipitation extremes towards the cold season in this region. Marelle et al. (2018) also found a shift towards the cold season for many regions in both CMIP5 models and regional models from the Coordinated Regional Downscaling Experiment (CORDEX). Furthermore, although climate models exhibit regional biases in precipitation extremes (Pfahl et al., 2017), Marelle et al. (2018) found that the CMIP5 and CORDEX models reproduce most aspects of the seasonality of precipitation extremes in the current climate when compared to gridded observations, which increases confidence in their future projections for changes in seasonality.

High-resolution, regional models have also shown a weaker response of precipitation extremes to climate change in JJA than DJF in Europe (Wood & Ludwig, 2020). This summer-winter contrast was also found in convection-permitting simulations of the Mediterranean (Pichelli et al., 2021) and the Contiguous United States (Prein et al., 2017), which is notable since convection-permitting simulations are better able to represent short-duration precipitation extremes (Prein et al., 2015). Precipitation extremes in JJA are known to be sensitive to how convection is represented (Chan et al., 2014; Prein et al., 2015; Ban et al., 2015; Kooperman et al., 2014), and caution is needed for projections in regions and seasons with significant mesoscale convective activity, particularly for sub-daily extremes. This emphasizes the importance of seeking observational evidence and robust physical mechanisms that may support projected seasonal changes in precipitation extremes.

Here, we focus on the summer-winter contrast in the fractional response of daily precipitation extremes to climate warming in the NH in CMIP5 models and gridded observations. We begin by describing the model output and observational data and the methods of analysis (Section 2). We then show that the JJA-DJF contrast is primarily due

104 to differences in the dynamic contribution between JJA and DJF, but that differences  
 105 in the thermodynamic contribution also play a role, particularly at high latitudes (Section  
 106 3). We further show that the negative dynamic contribution in JJA is strongly cor-  
 107 related in terms of model scatter and spatial pattern to decreases in mean near-surface  
 108 relative humidity over land and explore possible physical mechanisms for this negative  
 109 dynamic contribution (Section 4). Finally, we demonstrate that the summer-winter con-  
 110 trast is also evident in gridded observational datasets and CMIP5 simulations over the  
 111 historical period (Section 5), before giving our conclusions (Section 6).

## 112 2 Methods

113 We analyse changes over 1950–2100 under the historical and RCP8.5 scenarios for  
 114 CMIP5. All models are used that provide the required data (listed in Text S1). The scal-  
 115 ing and decomposition based on Eq. 1 is taken from Pfahl et al. (2017), and further de-  
 116 tails can be found there, but we repeat the key points of the calculation here. We chose  
 117 not to repeat their calculations with CMIP6 output because there is little improvement  
 118 in the simulation of daily precipitation extremes between CMIP5 and CMIP6 (Wehner  
 119 et al., 2020).

120 Daily surface precipitation was used to calculate the maximum daily precipitation  
 121 amount ( $Rx1day$ ) for JJA and DJF in each year. Daily-mean temperature and vertical  
 122 pressure velocity on all available pressure levels at the location and day of each daily-  
 123 maximum precipitation event ( $T_e$  and  $\omega_e$ , respectively) were then used to calculate the  
 124 full extreme precipitation scaling following Eq. 1 by performing a vertical integral over  
 125 all tropospheric levels with ascent ( $\omega_e < 0$ ). To calculate the thermodynamic contri-  
 126 bution, this analysis is repeated but with  $\omega_e$  replaced with its average over all years from  
 127 1950–2100.

128 To calculate the sensitivity to climate change, we first normalize  $Rx1day$  and the  
 129 full and thermodynamic scalings by dividing by their average over the historical period  
 130 (1950–2000). We then calculate the dynamic contribution as the difference between the  
 131 full and thermodynamic scaling. This approach to calculating the dynamic contribution  
 132 differs slightly from Pfahl et al. (2017), but yields similar results (e.g., compare our Fig.  
 133 1c with their Fig. S8d). We then regress these normalized time series against global- and  
 134 annual-mean surface temperature anomalies over 1950–2000 using the Theil-Sen estima-  
 135 tor to produce sensitivities in units of ( $\% K^{-1}$ ). The Theil-Sen estimator is a non-parametric  
 136 estimator which operates by choosing the median of the slopes of all lines through pairs  
 137 of points and is less sensitive to outliers than ordinary least-squares regression. This re-  
 138 gression approach has been shown to provide more robust results compared to taking  
 139 differences in multi-decadal means (Fischer et al., 2014). When presenting results for the  
 140 seasonal contrast (JJA–DJF), the sensitivities are calculated by differencing the normal-  
 141 ized JJA and DJF time series in each grid box, before regressing this ‘difference’ time  
 142 series against global-mean surface temperature anomalies for each model. Using a nor-  
 143 malization over a reference period can sometimes produce statistical biases for changes  
 144 in precipitation extremes (Donat et al., 2016; Sippel et al., 2017), but our results remain  
 145 largely unchanged when using the full 1950–2100 period for normalization (Fig. S2).

146 All analysis is performed on each model’s native grid, and then the sensitivities are  
 147 re-gridded to a uniform  $1^\circ \times 1^\circ$  grid before calculating multi-model statistics and zonal  
 148 means. Pfahl et al. (2017) noted previously that some models produce very low seasonal  
 149  $Rx1day$  at some grid points in the subtropics, which creates anomalously large extreme  
 150 precipitation sensitivities. Thus, when calculating multi-model or zonal means we ex-  
 151 clude grid boxes from models where the average seasonal  $Rx1day$  over the historical pe-  
 152 riod is less than  $0.5 \text{ mm day}^{-1}$ . Additionally, we found that the CMCC-CMS model pro-  
 153 duced unrealistically large changes in the thermodynamic contribution over Pakistan and

154 Afghanistan, and so for this model we exclude the region from  $29.5^{\circ}$  to  $32.5^{\circ}$  latitude  
 155 and  $60^{\circ}$  to  $68^{\circ}$  longitude.

156 We also analyse changes in seasonal Rx1day over the historical period over land  
 157 in observations and compare them to the same period in the CMIP5 simulations (com-  
 158 bining the historical and RCP8.5 simulations). We analyse the ‘extended’ NH summer  
 159 (MJJAS) and winter (NDJFM) seasons (as opposed to JJA and DJF) to improve the  
 160 signal-to-noise ratio and use data from 1950-2017, with the time-period chosen for max-  
 161 imum overlap with the CMIP5 data. For Rx1day observations, we focus on the HadEX3  
 162 gridded dataset (Dunn et al., 2020) which has a spatial resolution of  $1.25^{\circ} \times 1.875^{\circ}$ , but  
 163 we also show results for the GHCNDEX observational dataset over 1952-2018 (Donat  
 164 et al., 2013) which has a resolution of  $2.5^{\circ} \times 2.5^{\circ}$  in the supplement as a point of com-  
 165 parison. To calculate annual- and global-mean surface temperatures (including land and  
 166 ocean) from observations, we use the NOAA Merged Land-Ocean Surface Temperature  
 167 Analysis (Vose et al., 2012).

168 Sensitivities in  $\% \text{ K}^{-1}$  for the observations are calculated at each gridbox as de-  
 169 scribed earlier but requiring at least 45 years of data at that grid box and normalizing  
 170 by an average over all the years used. When analysing the summer-winter contrast (here,  
 171 MJAS-NDJFM) we require each grid box to have 45 years of data for both seasons in  
 172 each year, and we normalize each time series separately before differencing and then per-  
 173 forming the regression. CMIP5 data are subsampled to the observations in both space  
 174 and time. To reduce the influence of unforced variability and outliers, we then aggregate  
 175 the sensitivities into  $5^{\circ}$  latitude bands and calculate the median sensitivity across each  
 176 latitude band. We use bootstrapping to estimate the uncertainty due to inter-annual vari-  
 177 ability and the non-uniform spatial coverage of the observations. To do this we calcu-  
 178 late 10,000 bootstrap samples per latitude band, where each sample involves a random  
 179 choice of both the years used for each grid box to calculate the regression, and a ran-  
 180 dom choice of the grid boxes used to calculate the median sensitivity across the latitude  
 181 band. We then calculate the median sensitivity for each bootstrap sample, and then the  
 182 90% confidence interval across samples for each latitude band. Our conclusions are largely  
 183 insensitive to the size of the latitude bands and the number of bootstrap samples used,  
 184 except in the tropics where larger latitude bands can obscure seasonal migrations of the  
 185 ITCZ.

### 186 3 Summer-Winter contrast in CMIP5

187 Figure 1 shows the multi-model mean patterns of seasonal Rx1day sensitivity based  
 188 on the scaling Eq. 1 and its decomposition into thermodynamic and dynamic contribu-  
 189 tions for JJA, DJF and JJA-DJF. As found in previous studies, the thermodynamic con-  
 190 tribution is relatively uniform with robust agreement on the sign and the magnitude in  
 191 both seasons. In stark contrast, the dynamic contribution exhibits strong regional and  
 192 seasonal variations.

193 The NH extratropics show a strongly negative JJA-DJF contrast especially over  
 194 land (Fig. 1g). Over this region, the DJF response (Fig. 1d) is amplified by a positive  
 195 contribution from the dynamics (Fig. 1f) and a relatively strong thermodynamic con-  
 196 tribution particularly at high latitudes (Fig. 1e). On the other hand, the response dur-  
 197 ing JJA is ‘muted’, with much less multi-model agreement and with some regions (par-  
 198 ticularly Europe and the continental United States) exhibiting close to no change or even  
 199 negative responses of extreme precipitation to warming (Fig. 1a). This weak JJA response  
 200 arises predominantly due to the strongly negative dynamic contribution (Fig. 1c) which  
 201 cancels out the robust, positive increase due to the thermodynamic contribution (Fig.  
 202 1b). The negative dynamic contribution in JJA is particularly strong over land and parts  
 203 of the subtropical Atlantic. A land-ocean contrast in the dynamic contribution in JJA  
 204 is apparent when examining anomalies from the zonal-mean (Fig. S3), which show that

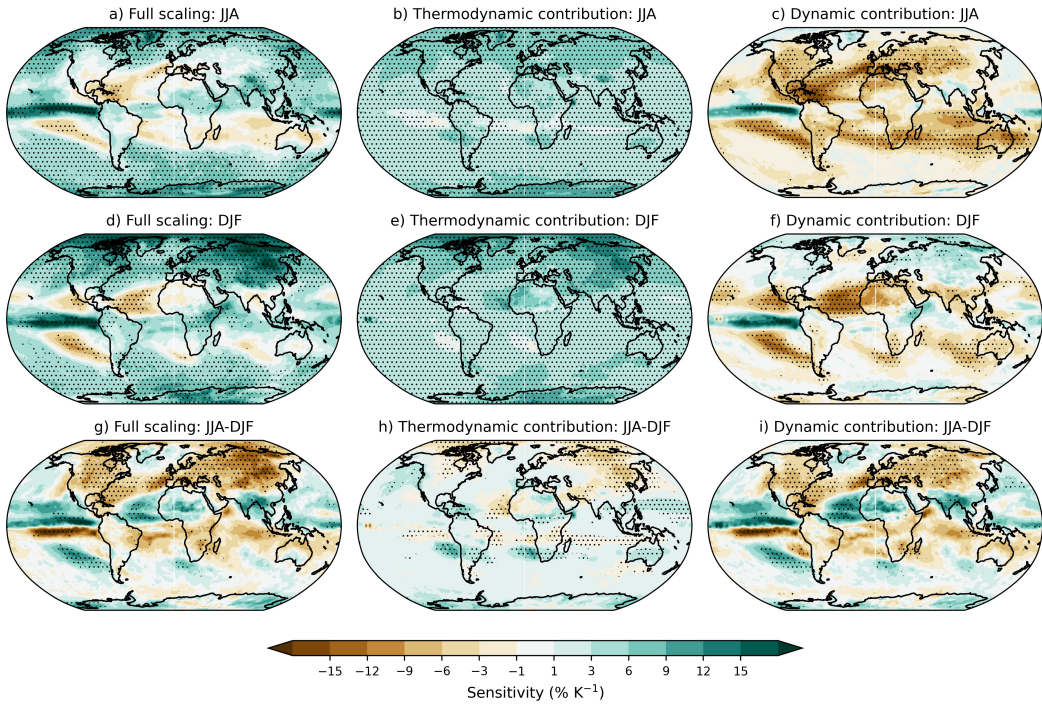


**Figure 1.** Multi-model mean Rx1day sensitivity over 1950-2100 according to the scaling Eq. 1 (a,d,g) and decomposition into (b,e,h) thermodynamic and (c,f,i) dynamic contributions for (a-c) JJA, (d-f) DJF and (e-i) JJA minus DJF, the summer-winter contrast. Stippling indicates where at least 90% of the models agree on the sign of the change.

205 the negative dynamic contribution extends further poleward over NH land as compared  
 206 to ocean. The combination of the very weak response in JJA and the amplified response  
 207 in DJF leads to the strong JJA-DJF difference in the response, particularly over NH mid-  
 208 latitude land. The dynamic contribution is responsible for most of the JJA-DJF differ-  
 209 ence, as illustrated by the similarity between Fig. 1g and i, but seasonal differences in  
 210 the thermodynamic contribution also play a role (Fig. 1h).

211 We next examine zonal-mean changes in the scaling decomposition over both land  
 212 and ocean and over land only (Fig. 2). The thermodynamic contribution is larger at higher  
 213 latitudes (e.g., Fig. 2b,e) and is partly responsible for the JJA-DJF contrast at NH mid-  
 214 latitude and high latitudes (Fig. 2c,f), implying a stronger thermodynamic contribution in  
 215 DJF than JJA. A stronger thermodynamic contribution is expected for the lower tem-  
 216 peratures in winter and at higher latitudes because percentage increases in  $\frac{d\alpha_s}{dp}|_{\theta^*}$  with  
 217 increasing temperature are larger at lower temperatures (O’Gorman & Schneider, 2009a).  
 218 It could also be argued that Arctic amplification of surface warming also plays a role,  
 219 and indeed the JJA-DJF contrast in the NH thermodynamic contribution is negligible  
 220 when we regress against zonal-mean temperature (Fig. S4). However, the stronger ther-  
 221 modynamic contribution at higher (and colder) latitudes is also found to occur even when  
 222 a globally uniform surface warming is imposed (O’Gorman et al., 2021) suggesting that  
 223 it is not tied to Arctic amplification. Additionally, previous studies have found there is  
 224 less warming of  $T_e$  than mean temperature at middle and high latitudes (e.g., Fig. S5  
 225 of O’Gorman and Schneider (2009a) or Fig. 8c of O’Gorman and Schneider (2009b)) which  
 226 suggests that normalizing by the local changes in zonal-mean temperature gives too much  
 227 emphasis to Arctic amplification.

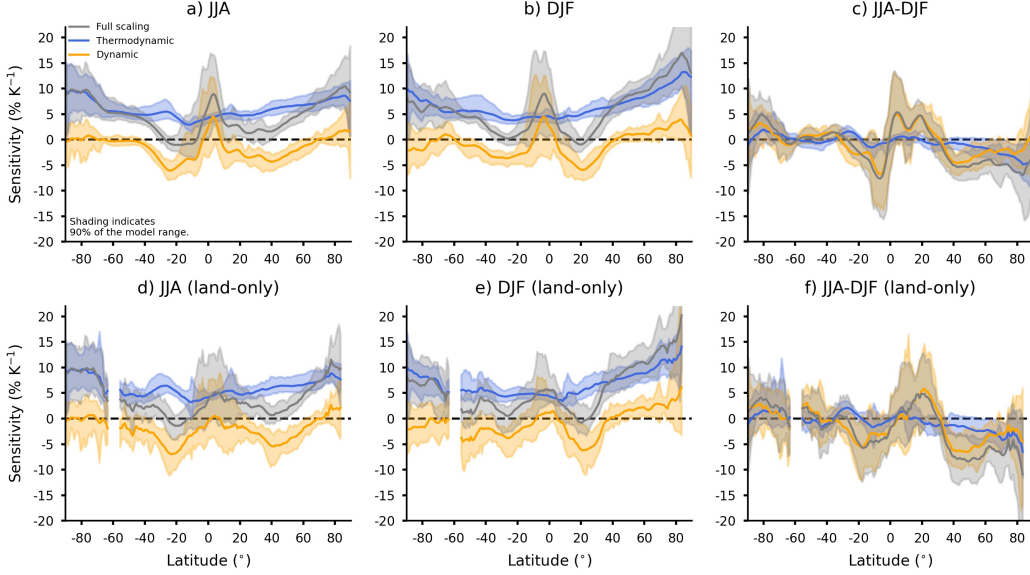


**Figure 2.** Zonal-mean of the Rx1day sensitivity over 1950-2100 according to the scaling and its decomposition into thermodynamic and dynamic contributions for (a) JJA, (b) DJF and (c) JJA-DJF. Lines indicate multi-model means and shading shows the 90% model range. Panels (d,e,f) show the same results but for over land only.

In the tropics, the zonal-mean results in Fig. 2 are consistent with amplification of precipitation extremes along the ITCZ region, which moves seasonally. This leads to a southward shift in precipitation extremes when considering the summer-winter contrast (Fig. 2c,f) because the ITCZ occurs further south in DJF than in JJA. These shifts are driven by the dynamic contribution as demonstrated by the similarity between the changes in the full scaling and the dynamic contribution in the tropics (gray and orange lines in Fig. 2c,f).

We have presented results in terms of percentage changes in ( $\% \text{ K}^{-1}$ ) as opposed to absolute changes ( $\text{mm day}^{-1} \text{ K}^{-1}$ ) because it is useful to consider the change in each season relative to what is expected for that season and because previous studies have also focused on percentage changes which are easier to relate to physical processes. Absolute changes also show a seasonal contrast for much of NH midlatitude land but not for some parts of Asia (Fig. S5g) or for zonal-mean quantities (Fig. S6f), because the thermodynamic contribution offsets the dynamic contribution when considering absolute changes. Thus, one additional advantage of considering percentage changes is that it provides a strong zonal-mean signal to look for in the observational record (Section 5).

#### 4 Physical mechanisms of the negative dynamic contribution in JJA

Dynamic weakening of precipitation extremes during JJA is a large contributor to the JJA-DJF contrast in the extratropical NH, particularly over land (Figs. 1c and 2d). Physically then, what mechanisms could be responsible for this dynamic weakening? Tandon et al. (2018) tackled this question using a three-term approximation of the QG- $\omega$  equation and found the weakening of extreme ascent was related to increases in the horizontal length scale of extreme ascent. However, Li and O’Gorman (2020) numerically inverted the QG- $\omega$  equation in extreme precipitation events and found that changes in eddy length were less important when all terms were retained in the QG- $\omega$  equation, although

they did not separately analyse extremes in JJA. Changes in moist static stability,  $\sigma_m$ , have also been found to be important in previous studies (Li & O’Gorman, 2020; Tandon et al., 2018), with an increase in  $\sigma_m$  associated with a weakening of ascent. Here, we calculate changes in moist static stability on the days of the extreme events following previous work (Text S2) and find that the changes in moist static stability are mostly consistent with the spatial pattern of the JJA dynamic contribution (Fig. S7), but they fail to capture the inter-model spread in projections over NH land (Fig. S8).

The fact that precipitation extremes in JJA over NH extratropical land are convective in nature motivates us to investigate a mechanism for the dynamic contribution in terms of changes in low-level relative humidity which would affect the environment for convection and the associated convective heating that amplifies large-scale ascent. Decreases in near-surface relative humidity ( $RH_{2m}$ ) over land are expected with global-warming because of the land-ocean warming contrast (Byrne & O’Gorman, 2016, 2018) and decreases in stomatal conductance (Cao et al., 2010; Berg et al., 2016). Furthermore, previous work has shown that decreases in relative humidity cause an increase in convective inhibition (CIN) that is particularly large over NH land in JJA (Chen et al., 2020).

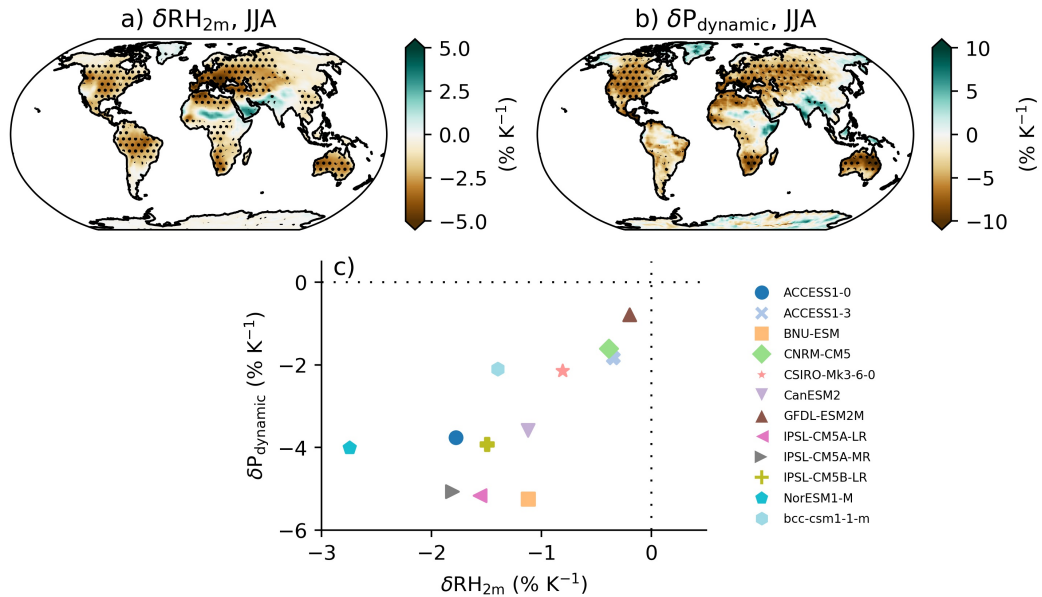


**Figure 3.** Sensitivity for JJA over 1950-2100 of (a) seasonal-mean near-surface relative humidity and (b) the dynamic contribution to changes in precipitation extremes. Results are shown for the 12 models that archived  $RH_{2m}$  and for which the dynamic contribution was calculated. Stippling indicates where 10 out the 12 models agree on the sign of the sensitivity. Panel (c) shows a scatter plot of the median sensitivities across land grid boxes in the latitude band 40–70°N for each model.

In Fig. 3 we compare the sensitivities of seasonal-mean  $RH_{2m}$  and the dynamic contribution to precipitation extremes during JJA for climate change over 1950-2100. The sensitivity of  $RH_{2m}$  is defined using regression analogously to the sensitivity of precipitation extremes and normalized by the 1950-2000 mean. There is strong agreement between the spatial pattern of the change in  $RH_{2m}$  and the dynamic contribution (Fig. 3a,b), with the models agreeing robustly on strong decreases in relative humidity and a negative dynamic contribution over similar regions of the globe. Furthermore, Fig. 3c shows

277 that models with a stronger decrease in JJA  $\text{RH}_{2m}$  also tend to have a stronger negative  
 278 dynamic contribution when averaged over NH midlatitude land. The link between  
 279 the dynamic contribution and  $\text{RH}_{2m}$  is not as strong in individual model runs (Fig. S9  
 280 and S10), potentially due to unforced variability in precipitation extremes and other mech-  
 281 anisms which act to change  $\omega_e$  in precipitation extremes but are not robust across mod-  
 282 els. Changes in  $\text{RH}_{2m}$  on the day of the event are weaker but are nonetheless strongly  
 283 correlated with the dynamic contribution (Fig. S11).

284 The details of the mechanism by which decreases in relative humidity inhibit con-  
 285 vective heating in extreme precipitation events requires further study, ideally with a cloud-  
 286 resolving model. One possibility is through increases in convective inhibition (CIN), and  
 287 we find that seasonal-mean CIN increases are correlated with the dynamic contribution  
 288 for both the spatial pattern and inter-model scatter (Text S3, Fig. S12). However, while  
 289 CIN on the day of the extreme precipitation event ( $\text{CIN}^e$ ) also increases, these changes  
 290 are not strongly correlated with the dynamic contribution in terms of inter-model scat-  
 291 ter (see Figs. S13-14 and discussion in Text S3). Thus, low-level relative humidity de-  
 292 creases may be inhibiting convection, but CIN on the day of the event is not clearly cap-  
 293 turing this effect. Relative humidity higher up in the troposphere on the day of the event  
 294 also decrease over land, but these changes are not as well correlated with the dynamic  
 295 contribution and may be caused by the changes in vertical velocity (Fig. S15, S16).

296 The relationship between changes in mean relative humidity and the negative dy-  
 297 namic contribution to changes in extreme precipitation in JJA (Fig. 3) is notable in that  
 298 it links changes in a mean quantity to changes in an extreme statistic. Such a link is po-  
 299 tentially very useful since mean quantities can be easier to observationally constrain than  
 300 extremes. The decrease in relative humidity occurs only over land, and factors such as  
 301 the changes in moist static stability discussed earlier (Li & O’Gorman, 2020; Tandon et  
 302 al., 2018), a general weakening of the extratropical storm track in NH JJA (O’Gorman,  
 303 2010; Gertler & O’Gorman, 2019), or the poleward expansion of the Hadley cells in the  
 304 subtropics (Pfahl et al., 2017; Norris et al., 2020) may also influence the dynamic con-  
 305 tribution over land and ocean.

306 In NH DJF, there is not a connection between changes in  $\text{RH}_{2m}$  and the dynamic  
 307 contribution (Fig. S17), which we hypothesize is because daily precipitation extremes  
 308 in DJF are controlled to a greater extent by large-scale dynamics as compared to the strongly  
 309 convective extremes in JJA.

310 Interestingly, there is also a negative dynamic contribution over the Southern Hemi-  
 311 sphere over both land and ocean in JJA (Fig. 1c). This negative dynamic contribution  
 312 does not show as clear a land-ocean contrast and primarily occurs at lower latitudes as  
 313 compared to the negative dynamic contribution in the NH, and thus we hypothesize it  
 314 may be more strongly influenced by factors such as Hadley cell expansion (Pfahl et al.,  
 315 2017; Norris et al., 2020).

## 316 5 Observed and modelled trends over the historical period

317 Given the difficulty in correctly representing convection in models, we next turn  
 318 our attention to gridded observations of precipitation extremes. Figure 4 shows the sen-  
 319 sitivity of daily precipitation extremes from HadEX3 observations and CMIP5 models  
 320 to warming over 1950-2017 for boreal summer (MJJAS) and extended winter (NDJFM),  
 321 and the seasonal contrast (MJJAS-NDJFM). The results are expressed as medians for  
 322 each 5° latitude bands (see Section 2). For the NH extratropics, the observed sensitiv-  
 323 ities are positive in both MJJAS and NDJFM, and there is a clear summer-winter con-  
 324 trast with lower sensitivities in MJJAS than NDJFM (Fig.4a,b,c). The seasonal contrast  
 325 is also evident when looking at maps of the sensitivities, but as expected there is con-  
 326 siderable noise when considering sensitivities for a period of this length in individual grid-

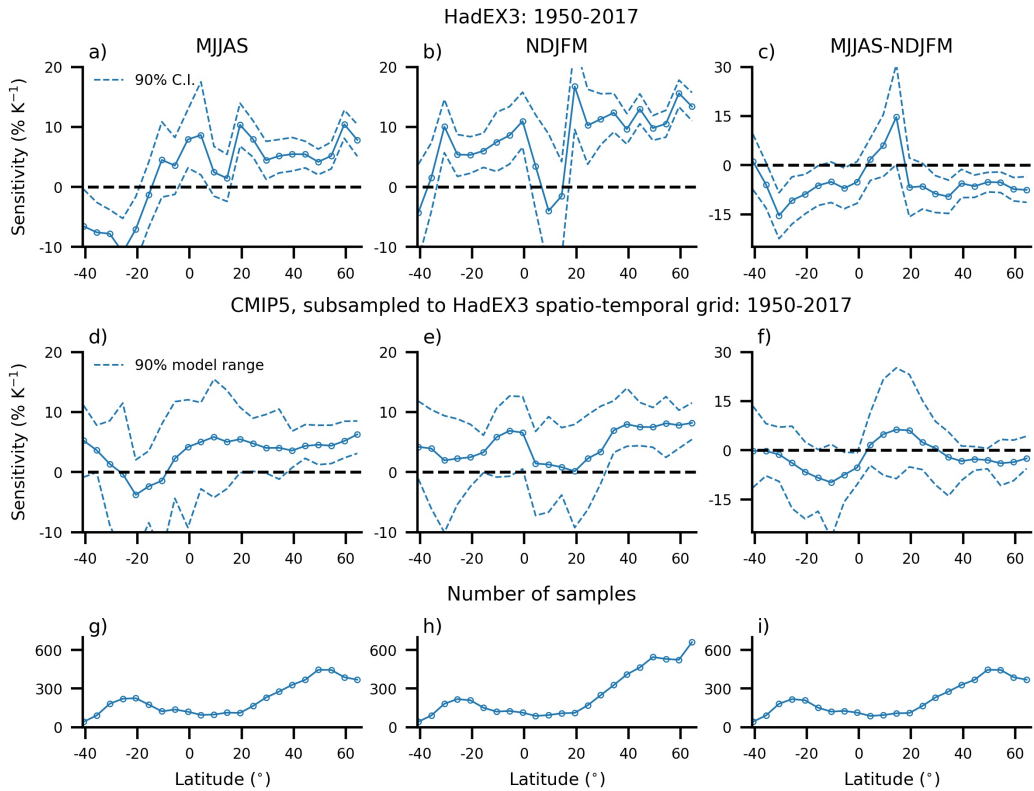


**Figure 4.** The sensitivity of Rx1day to warming over 1950-2017 in MJJAS (a,d), NDJFM (b,e) and MJJAS-NDJFM (c,f) for the HadEX3 dataset (a,b,c) and CMIP5 simulations subsampled to the HadEX3 dataset (d,e,f). Solid lines show the median sensitivity across the  $5^{\circ}$  latitude band. Dashed lines show the 90% confidence interval for HadEX3 and 90% of the model spread for CMIP5. The total number of samples included in each latitude band is also shown (g,h,i) which is the same for both the observations and the simulations.

327 boxes (Fig.S18 a,b,c). The NH extratropical summer-winter contrast is also present in  
 328 the CMIP5 models over the same historical period (Fig.4 d,e,f).

329 We next quantify the NH midlatitude response by averaging the sensitivities over  
 330 land between  $30\text{--}70^{\circ}\text{N}$  with area-weighting. For the observations, the mean NH sensitivity  
 331 is  $5.6\text{ \% K}^{-1}$  for MJJAS,  $11.6\text{ \% K}^{-1}$  for NDJFM, and  $-7.2\text{ \% K}^{-1}$  for MJJAS-  
 332 NDJFM. For the CMIP5 models over the same period, the multimodel-mean sensitivity  
 333 and full model range are  $4.4\text{ \% K}^{-1}$  ( $2.1$  to  $9.1\text{ \% K}^{-1}$ ) for MJJAS,  $7.0\text{ \% K}^{-1}$  ( $4.7$   
 334 to  $10.8\text{ \% K}^{-1}$ ) for NDJFM, and  $-2.4\text{ \% K}^{-1}$  ( $0.6$  to  $-8.4\text{ \% K}^{-1}$ ) for MJJAS-NDJFM.  
 335 Thus, while the models and observations show similar sensitivities during MJJAS, none  
 336 of the models capture the very strong observed sensitivity for NDJFM. As a result, while  
 337 the observed MJJAS-NDJFM contrast lies within the model range, the multi model-mean  
 338 value is smaller in magnitude than the value in observations. The smaller magnitude of  
 339 the sensitivity in the multimodel mean than in observations may be related to unforced  
 340 internal variability, which is reduced by considering the multimodel mean but is likely  
 341 to be still important in observations. Despite this, most but not all models (15/18) give  
 342 a negative MJJAS-NDJFM contrast for this period, consistent with the observations.

343 GHCNDEX has a coarser spatial resolution and fewer grid boxes with data com-  
 344 pared to HadEX3, particularly in the tropics, but we find similar changes in seasonal Rx1day

345 over the Northern Hemisphere (Figs. S18 and S19), which strengthens our confidence  
 346 in the results. Similar results are also found when the CMIP5 data are not subsampled  
 347 to the observations (Figure S20), which suggests that missing grid points in the obser-  
 348 vations are not affecting our conclusions. The robust presence of the MJJAS-NDJFM  
 349 contrast in observed trends over the historical period supports the contrast found in ear-  
 350 lier sections.

## 351 6 Conclusions

352 In this study we have demonstrated that CMIP5 models project a robust summer-  
 353 winter contrast in the response of precipitation extremes to warming over Northern Hem-  
 354 isphere midlatitude land, with considerably weaker percentage changes in JJA than DJF.  
 355 We have also shown that this summer-winter contrast is evident in gridded observations  
 356 over the historical period, which strengthens our confidence in the future projections.  
 357 CMIP5 simulations over the historical period also show a summer-winter contrast that  
 358 occurs in 15/18 models, and the model range includes the observed value of this contrast.

359 Furthermore, we have used a simple, physical scaling to help explain the cause of  
 360 the summer-winter contrast in changes in precipitation extremes. The contrast is pri-  
 361 marily caused by the dynamic contribution (related to changes in extreme ascent) with  
 362 strongly negative dynamic contribution in JJA and a weakly positive dynamic contri-  
 363 bution in DJF. The negative dynamic contribution in JJA is strong over NH extratrop-  
 364 ical land, and we show it is correlated with decreases in near-surface relative humidity  
 365 in terms of spatial pattern and inter-model scatter. The negative dynamic contribution  
 366 is also correlated with increases in seasonal CIN but less so for CIN on the day of the  
 367 extreme precipitation event, and thus further work is required to investigate the dynam-  
 368 ical mechanism involved and demonstrate causality.

369 The thermodynamic contribution to changes in precipitation extremes also helps  
 370 to amplify the response in winter over summer, particularly over high latitudes. We have  
 371 focused on percentage seasonal changes because they may be more relevant for impacts  
 372 in a given season and to better connect with physical mechanisms. If absolute rather than  
 373 percentage changes in precipitation extremes are considered, the thermodynamic con-  
 374 tribution is larger in summer than winter, and this offsets the JJA-DJF contrast in the  
 375 dynamic contribution, although the contrast is still evident over much of NH midlati-  
 376 tude land (Fig. S5).

377 Future work could build on our observational analysis by performing a formal de-  
 378 tection and attribution analysis of the seasonal difference in trends of precipitation ex-  
 379 tremes. Future work could also build more understanding of the positive dynamic con-  
 380 tribution in the NH extratropics in winter, which is important as DJF is the season of  
 381 maximum daily precipitation in many regions (Marelle et al., 2018). Future work could  
 382 also investigate the detailed mechanism of the link between changes in relative humid-  
 383 ity and precipitation extremes in summer using idealized experiments in cloud-resolving  
 384 models, which would also help to establish the physical reliability of this link. Given the  
 385 potential importance of decreases in relative humidity over land for convection and pre-  
 386 cipitation extremes, it would be helpful to develop an emergent constraint for the mag-  
 387 nitude of the expected decrease, although this may be difficult to the extent that it de-  
 388 pends both on the land-ocean warming contrast and the plant physiological response to  
 389 increased  $\text{CO}_2$  levels.

## 390 7 Open Research

391 Processed observational and climate model data supporting the conclusions in this  
 392 study can be found at <https://doi.org/10.5281/zenodo.6341493>.

393 **Acknowledgments**

394 A.I.L.W. acknowledges funding from the Natural Environment Research Council,  
 395 Oxford DTP, award NE/S007474/1 and the Laidlaw Research and Leadership Programme.  
 396 P.A.O'.G. acknowledges support from NSF awards AGS-1552195 and AGS-1749986.

397 We acknowledge the World Climate Research Programme's Working Group on Cou-  
 398 pled Modelling, which is responsible for CMIP, and we thank the climate modeling groups  
 399 for producing and making available their model output. We thank Stephan Pfahl for gen-  
 400 erously providing the CMIP5 scaling data used for this study and Ziwei Li for helpful  
 401 discussions. A.I.L.W. thanks Makayla Haussler for moral support and input on the fig-  
 402 ures.

403 **References**

404 Ban, N., Schmidli, J., & Schär, C. (2015). Heavy precipitation in a changing cli-  
 405 mate: Does short-term summer precipitation increase faster? *Geophysical Re-*  
 406 *search Letters*, 42(4), 1165–1172. doi: 10.1002/2014GL062588

407 Berg, A., Findell, K., Lintner, B., Giannini, A., Seneviratne, S. I., van den Hurk, B.,  
 408 ... Milly, P. C. D. (2016). Land–atmosphere feedbacks amplify aridity increase  
 409 over land under global warming. *Nature Climate Change*, 6(9), 869–874. doi:  
 410 10.1038/nclimate3029

411 Byrne, M. P., & O'Gorman, P. A. (2016). Understanding decreases in land relative  
 412 humidity with global warming: Conceptual model and GCM simulations. *Jour-*  
 413 *nal of Climate*, 29(24), 9045–9061. doi: 10.1175/JCLI-D-16-0351.1

414 Byrne, M. P., & O'Gorman, P. A. (2018). Trends in continental temperature  
 415 and humidity directly linked to ocean warming. *Proceedings of the National*  
 416 *Academy of Sciences*, 115(19), 4863–4868. doi: 10.1073/pnas.1722312115

417 Cao, L., Bala, G., Caldeira, K., Nemani, R., & Ban-Weiss, G. (2010). Importance  
 418 of carbon dioxide physiological forcing to future climate change. *Proceedings*  
 419 *of the National Academy of Sciences*, 107(21), 9513–9518. doi: 10.1073/pnas  
 420 .0913000107

421 Chan, S. C., Kendon, E. J., Fowler, H. J., Blenkinsop, S., Roberts, N. M., & Ferro,  
 422 C. A. T. (2014). The value of high-resolution met office regional climate mod-  
 423 els in the simulation of multihourly precipitation extremes. *Journal of Climate*,  
 424 27(16), 6155–6174. doi: 10.1175/JCLI-D-13-00723.1

425 Chen, J., Dai, A., Zhang, Y., & Rasmussen, K. L. (2020). Changes in convective  
 426 available potential energy and convective inhibition under global warming.  
 427 *Journal of Climate*, 33(6), 2025–2050. doi: 10.1175/JCLI-D-19-0461.1

428 Diffenbaugh, N. S., & Burke, M. (2019). Global warming has increased global eco-  
 429 nomic inequality. *Proceedings of the National Academy of Sciences*, 116(20),  
 430 9808–9813. doi: 10.1073/pnas.1816020116

431 Donat, M. G., Alexander, L. V., Yang, H., Durre, I., Vose, R., Dunn, R. J. H., ...  
 432 Kitching, S. (2013). Updated analyses of temperature and precipitation  
 433 extreme indices since the beginning of the twentieth century: The HadEX2  
 434 dataset. *Journal of Geophysical Research: Atmospheres*, 118(5), 2098–2118.  
 435 doi: 10.1002/jgrd.50150

436 Donat, M. G., Lowry, A. L., Alexander, L. V., O'Gorman, P. A., & Maher, N.  
 437 (2016). More extreme precipitation in the world's dry and wet regions. *Nature*  
 438 *Climate Change*, 6(5), 508–513. doi: 10.1038/nclimate2941

439 Dunn, R. J. H., Alexander, L. V., Donat, M. G., Zhang, X., Bador, M., Herold, N.,  
 440 ... Bin Hj Yussof, M. N. (2020). Development of an updated global land  
 441 in situ-based data set of temperature and precipitation extremes: HadEX3.  
 442 *Journal of Geophysical Research: Atmospheres*, 125(16), e2019JD032263. doi:  
 443 10.1029/2019JD032263

444 Fischer, E. M., Sedláček, J., Hawkins, E., & Knutti, R. (2014). Models agree on  
 445 forced response pattern of precipitation and temperature extremes. *Geophysical Research Letters*, 41(23), 8554–8562. doi: 10.1002/2014GL062018

446 Gertler, C. G., & O’Gorman, P. A. (2019). Changing available energy for extra-  
 447 tropical cyclones and associated convection in northern hemisphere summer.  
 448 *Proceedings of the National Academy of Sciences*, 116(10), 4105–4110. doi:  
 449 10.1073/pnas.1812312116

450 Kharin, V. V., Zwiers, F. W., Zhang, X., & Wehner, M. (2013). Changes in tem-  
 451 perature and precipitation extremes in the CMIP5 ensemble. *Climatic Change*,  
 452 119(2), 345–357. doi: 10.1007/s10584-013-0705-8

453 Kirschbaum, D., Adler, R., Adler, D., Peters-Lidard, C., & Huffman, G. (2012).  
 454 Global distribution of extreme precipitation and high-impact landslides in 2010  
 455 relative to previous years. *Journal of Hydrometeorology*, 13(5), 1536–1551. doi:  
 456 10.1175/JHM-D-12-02.1

457 Knapp, A. K., Beier, C., Briske, D. D., Classen, A. T., Luo, Y., Reichstein, M., ...  
 458 Weng, E. (2008). Consequences of more extreme precipitation regimes for  
 459 terrestrial ecosystems. *BioScience*, 58(9), 811–821.

460 Kooperman, G. J., Pritchard, M. S., & Somerville, R. C. J. (2014). The re-  
 461 sponse of US summer rainfall to quadrupled CO<sub>2</sub> climate change in conven-  
 462 tional and superparameterized versions of the NCAR community atmosphere  
 463 model. *Journal of Advances in Modeling Earth Systems*, 6(3), 859–882. doi:  
 464 10.1002/2014MS000306

465 Li, Z., & O’Gorman, P. A. (2020). Response of vertical velocities in extratropical  
 466 precipitation extremes to climate change. *Journal of Climate*, 33(16), 7125–  
 467 7139. doi: 10.1175/JCLI-D-19-0766.1

468 Marelle, L., Myhre, G., Hodnebrog, , Sillmann, J., & Samset, B. H. (2018). The  
 469 changing seasonality of extreme daily precipitation. *Geophysical Research Letters*,  
 470 45(20), 11,352–11,360. doi: 10.1029/2018GL079567

471 Norris, J., Chen, G., & Li, C. (2020). Dynamic amplification of subtropical extreme  
 472 precipitation in a warming climate. *Geophysical Research Letters*, 47(14),  
 473 e2020GL087200. doi: <https://doi.org/10.1029/2020GL087200>

474 O’Gorman, P. A., & Schneider, T. (2009a). The physical basis for increases in pre-  
 475 cipitation extremes in simulations of 21st-century climate change. *Proceedings  
 476 of the National Academy of Sciences*, 106(35), 14773–14777. doi: 10.1073/pnas  
 477 .0907610106

478 O’Gorman, P. A. (2010). Understanding the varied response of the extratropical  
 479 storm tracks to climate change. *Proceedings of the National Academy of Sci-  
 480 ences*, 107(45), 19176–19180. doi: 10.1073/pnas.1011547107

481 O’Gorman, P. A. (2015). Precipitation extremes under climate change. *Current Cli-  
 482 mate Change Reports*, 1(2), 49–59. doi: 10.1007/s40641-015-0009-3

483 O’Gorman, P. A., Li, Z., Boos, W. R., & Yuval, J. (2021). Response of extreme  
 484 precipitation to uniform surface warming in quasi-global aquaplanet simu-  
 485 lations at high resolution. *Philosophical Transactions of the Royal Society A:  
 486 Mathematical, Physical and Engineering Sciences*, 379(2195), 20190543. doi:  
 487 10.1098/rsta.2019.0543

488 O’Gorman, P. A., & Schneider, T. (2009b). Scaling of precipitation extremes over  
 489 a wide range of climates simulated with an idealized gcm. *Journal of Climate*,  
 490 22(21), 5676 - 5685. doi: 10.1175/2009JCLI2701.1

491 Pfahl, S., O’Gorman, P. A., & Fischer, E. M. (2017). Understanding the regional  
 492 pattern of projected future changes in extreme precipitation. *Nature Climate  
 493 Change*, 7(6), 423–427. doi: 10.1038/nclimate3287

494 Pichelli, E., Coppola, E., Sobolowski, S., Ban, N., Giorgi, F., Stocchi, P., ...  
 495 Vergara-Temprado, J. (2021). The first multi-model ensemble of regional  
 496 climate simulations at kilometer-scale resolution part 2: historical and future  
 497 simulations of precipitation. *Climate Dynamics*, 56(11), 3581–3602. doi:  
 498

499 10.1007/s00382-021-05657-4

500 Prein, A. F., Langhans, W., Fosser, G., Ferrone, A., Ban, N., Goergen, K., ... Le-  
501 ung, R. (2015). A review on regional convection-permitting climate modeling:  
502 Demonstrations, prospects, and challenges. *Reviews of Geophysics*, 53(2),  
503 323–361. doi: 10.1002/2014RG000475

504 Prein, A. F., Rasmussen, R. M., Ikeda, K., Liu, C., Clark, M. P., & Holland, G. J.  
505 (2017). The future intensification of hourly precipitation extremes. *Nature  
506 Climate Change*, 7(1), 48–52. doi: 10.1038/nclimate3168

507 Sippel, S., Zscheischler, J., Heimann, M., Lange, H., Mahecha, M. D., van Old-  
508 enborgh, G. J., ... Reichstein, M. (2017). Have precipitation extremes  
509 and annual totals been increasing in the world's dry regions over the last  
510 60 years? *Hydrology and Earth System Sciences*, 21(1), 441–458. doi:  
511 10.5194/hess-21-441-2017

512 Tandon, N. F., Nie, J., & Zhang, X. (2018). Strong influence of eddy length on bo-  
513 real summertime extreme precipitation projections. *Geophysical Research Let-  
514 ters*, 45(19), 10,665–10,672. doi: 10.1029/2018GL079327

515 Taylor, K. E., Stouffer, R. J., & Meehl, G. A. (2012). An overview of CMIP5 and  
516 the experiment design. *Bulletin of the American Meteorological Society*, 93(4),  
517 485–498. doi: 10.1175/BAMS-D-11-00094.1

518 Vose, R. S., Arndt, D., Banzon, V. F., Easterling, D. R., Gleason, B., Huang, B.,  
519 ... Wuertz, D. B. (2012). NOAA's merged land–ocean surface temperature  
520 analysis. *Bulletin of the American Meteorological Society*, 93(11), 1677–1685.  
521 doi: 10.1175/BAMS-D-11-00241.1

522 Wehner, M., Gleckler, P., & Lee, J. (2020). Characterization of long period return  
523 values of extreme daily temperature and precipitation in the CMIP6 models:  
524 Part 1, model evaluation. *Weather and Climate Extremes*, 30, 100283. doi:  
525 10.1016/j.wace.2020.100283

526 Wood, R. R., & Ludwig, R. (2020). Analyzing internal variability and forced re-  
527 sponse of subdaily and daily extreme precipitation over europe. *Geophysical  
528 Research Letters*, 47(17), e2020GL089300. doi: 10.1029/2020GL089300